Available online at www.sciencedirect.com
ScienceDirect
Journal of the European Ceramic Society 29 (2009) 337–345
www.elsevier.com/locate/jeurceramsoc

Single crystalline mullite fibres obtained by the internal crystallisation method: Microstructure and creep resistance

S.T. Mileiko *, A.V. Serebryakov, V.M. Kiiko, A.A. Kolchin, V.N. Kurlov, N.I. Novokhatskaya

Solid State Physics Institute of the Russian Academy of Sciences, Chernogolovka 142432, Moscow District, Russia

Received 2 April 2008; received in revised form 25 June 2008; accepted 26 June 2008

Abstract

Single crystalline mullite fibres, which are expected to be an excellent reinforcement for high temperature composite materials, can be produced by using the internal crystallisation method. The present paper sheds light to mechanisms of crystallisation of mullite fibres under conditions of the internal crystallisation method, which is actually crystallisation of a melt in the continuous channels of a molybdenum carcass. Mullite occurs to appear close to 2:1 composition independent of the composition of the melt. Inclusions of a silica-based glassy phase are also present on the periphery of a fibre. The glassy phase yields a decrease in the creep resistance of mullite fibres at temperatures above 1500 °C. Still, the fibres obtained from the raw material with the Al_2O_3/SiO_2 molar ratio of 2.05 have excellent creep resistance at a temperature of 1400 °C and fairly high creep resistance at 1500 °C.

Keywords: Microstructure-final; Mullite; Creep; Structural applications; Internal crystallisation method

1. Introduction

Mullite has been intensively studied during the last decades because both poly- and single-crystalline forms of it are characterised by attractive mechanical properties at high temperatures.[1,2] An important obstacle on a way to use both these forms of mullite as structural materials for high temperature applications is its inherent brittleness. Hence, fibrous composites of a special structure are needed to make mullite-based materials to be sufficiently tough. Examples of mullite-based-fibre/mullite-matrix composites are known.[3,4] Polycrystalline fibres (e.g. 3M Nextel 720) used in those composites limit their creep resistance by a temperature of about 1200 °C.[5] The only known experimental point obtained in testing a single crystalline mullite specimen under compression published long time ago[1] makes obtaining single crystalline mullite fibres an important technical problem. There are known attempts to obtain them by using usual approaches.[6]

However, a number of the reasons including a complicated phase diagram of the alumina–silica system,[7] which is certainly not sufficiently well established, as well as too different values of the saturated vapour pressure of alumina and silica[8] set serious problems in crystallising the fibres from the melt while using well-known crystallisation methods, such as EFG[9] and LHPG,[10] normally employed to produce single crystalline oxide fibres. A technique called the internal crystallisation method (ICM)[11,12] allows producing a bundle of oxide rods-like fibres under conditions that make easier to crystallise complex oxides including single crystalline mullite.[13,14] Yet, up to now the fibre microstructure has not been studied in all the details. Mechanisms of crystallisation of the fibres are not clear. Creep characteristics of single crystalline mullite fibres have not been measured. The present paper aims to shed light on these aspects of single crystalline mullite fibres obtained by the internal crystallisation method.

2. Fabrication of the fibres

A schematic of the method has been described in details in previous publications.[12–14] Hence, here just a brief description of it is suitable. A molybdenum carcass with continuous channels in it, which is easily prepared by diffusion bonding of an assemblage of wires and foils is infiltrated with an oxide melt by the capillary force. The melt is then crystallised in the channels

* Corresponding author.
E-mail address: mileiko@issp.ac.ru (S.T. Mileiko).

0955-2219/$ – see front matter © 2008 Elsevier Ltd. All rights reserved.
doi:10.1016/j.jeurceramsoc.2008.06.022

to form fibres. Finally, the fibres are freed from the molybdenum carcass by dissolving molybdenum in a mixture of acids. A special cross-sectional shapes of the fibres are shown in a series of the micrographs presented below to illustrate fibre microstructures (see Figs. 1–4). The carcasses in the present study have the length of about 65 mm and the cross-section of about 5 mm × 5 mm. Characteristic size of a fibre cross-section is about 0.1 mm.

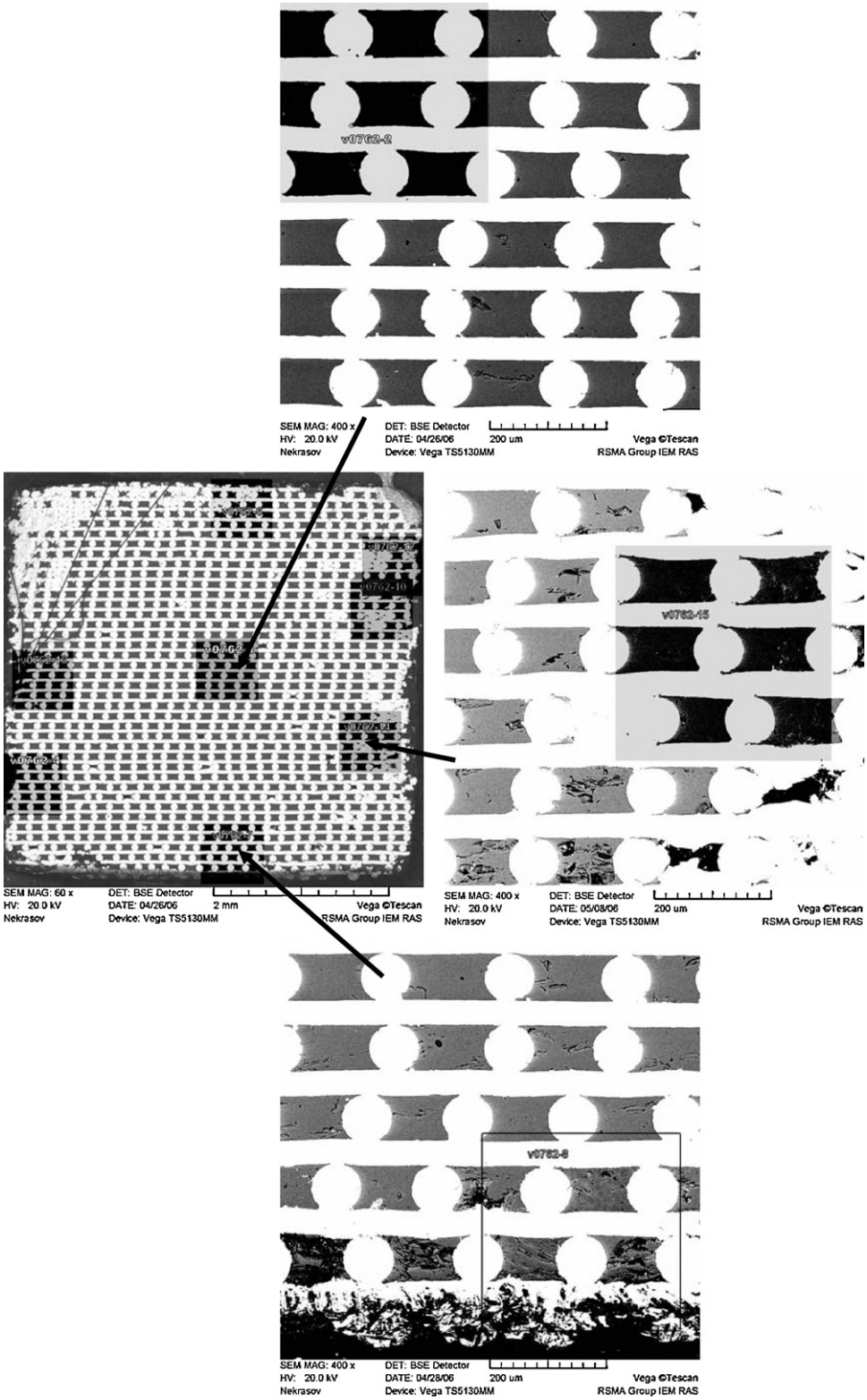

Fig. 1. Typical fibres in a cross-section of block V0762 corresponding to a steady state growth. The cross-section is taken at the middle length of the block. The precursor composition corresponds to $n = 2.05$.

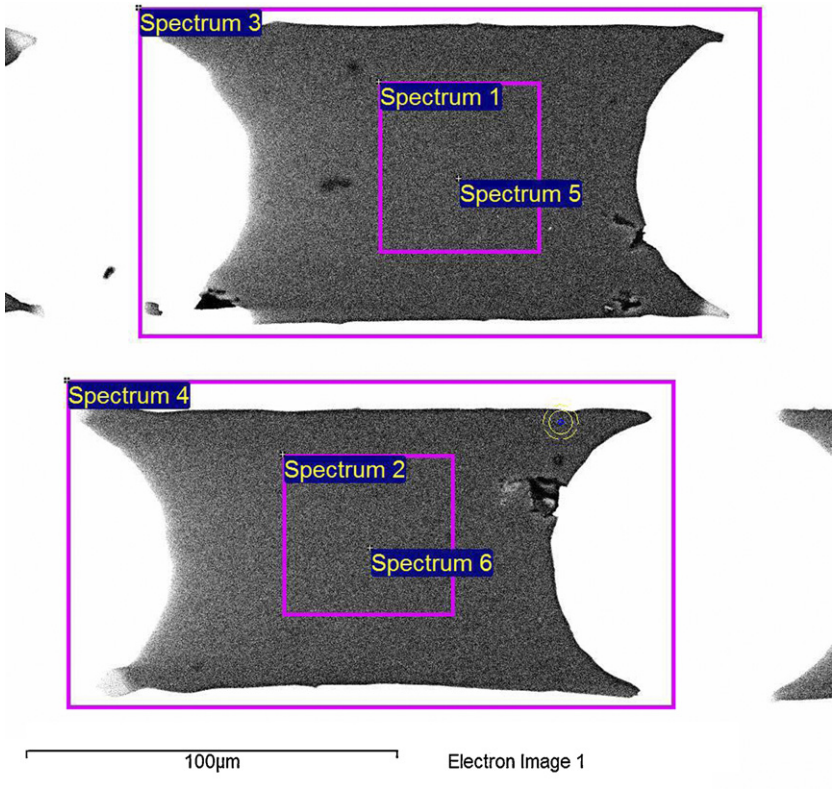

Fig. 2. A central portion of the block cross-section presented in Fig. 1 analysed by scanning by electron beam on the areas marked and at the points shown (see Table 1).

To study specific features of crystallisation of the melt containing a mixture of Al_2O_3 and SiO_2, a number of the raw compositions, $n{\cdot}Al_2O_3{:}SiO_2$, were used with the value of $n = 1.5$, 1.8 and 2.05. The lower value corresponds to 3:2 mullite, the upper one is close to 2:1 mullite, which is usually crystallised from the melt. Experiments with the composition corresponding to $n < 2$ allow revealing crystallisation mechanisms of the fibres.

Alumina and silica powders of a grain size of about 1 μm are mixed in ethanol for 8 h, then ethanol is evaporated and the mixture is pressed at room temperature to obtain a tablet, which is undergone to sintering at a temperature of 1300 °C for 3 h in air.

The tablets are melted in a molybdenum crucible, then the molybdenum carcass is inserted into the melt, which infiltrates the carcass by capillary force, and oxide/molybdenum block is being pulled into the cold zone of a furnace. Crystallisation of the melt in the channels of the carcass yields the fibres to be finally extracted from the block by dissolution of molybdenum in an acid. The crystallisation process is conducted in argon gas atmosphere. Before infiltration the melt is kept in a molybdenum crucible for up to 20 min to ensure a homogeniouty of the melt. Pulling rates of the oxide/molybdenum block during the crystallisation process were between 50 and 300 mm/h.

Mullite is known as crystallising from the melt in the *c*-axis direction. Still, to be sure that it is true with regard to fibres obtained by ICM, some fibres were taken randomly and their crystallographic orientation was determined by X-ray method. The fibre axis occurred to concise with the *c*-axis of 2:1 mullite.[1]

3. Microstructure

The fibre microstructure has been expected to depend on the composition of the melt and pulling rate; it occurs also that it changes along the length of an oxide/molybdenum block. Normally the microstructure changes rather quickly in the upper portion of the block where crystallisation starts and then remains fairly unchanged; so it is convenient to divide the block into two regions, that of a transient microstructure and that formed at a steady crystal growth. We will start with the steady state growth since this stage yields the fibres of nearly single-crystalline structure and then will come to the beginning of the process to trace a way to reach single crystallinity of the fibre. The study was performed by using X-ray microanalysis and scanning electron microscopy.

3.1. Experimental methods

Fully PC-controlled Scanning Electron Microscope VEGA TS 5130MM equipped with both detecting devices for secondary (SE) and backscatter (BSE) electrons on YAG-crystals

[1] X-ray diffraction experiment conducted by Dr. I.M. Shmyt'ko also reveals single crystallinity. The fibre axis nearly coincides with the *c*-axis of the orthorhombic crystal.

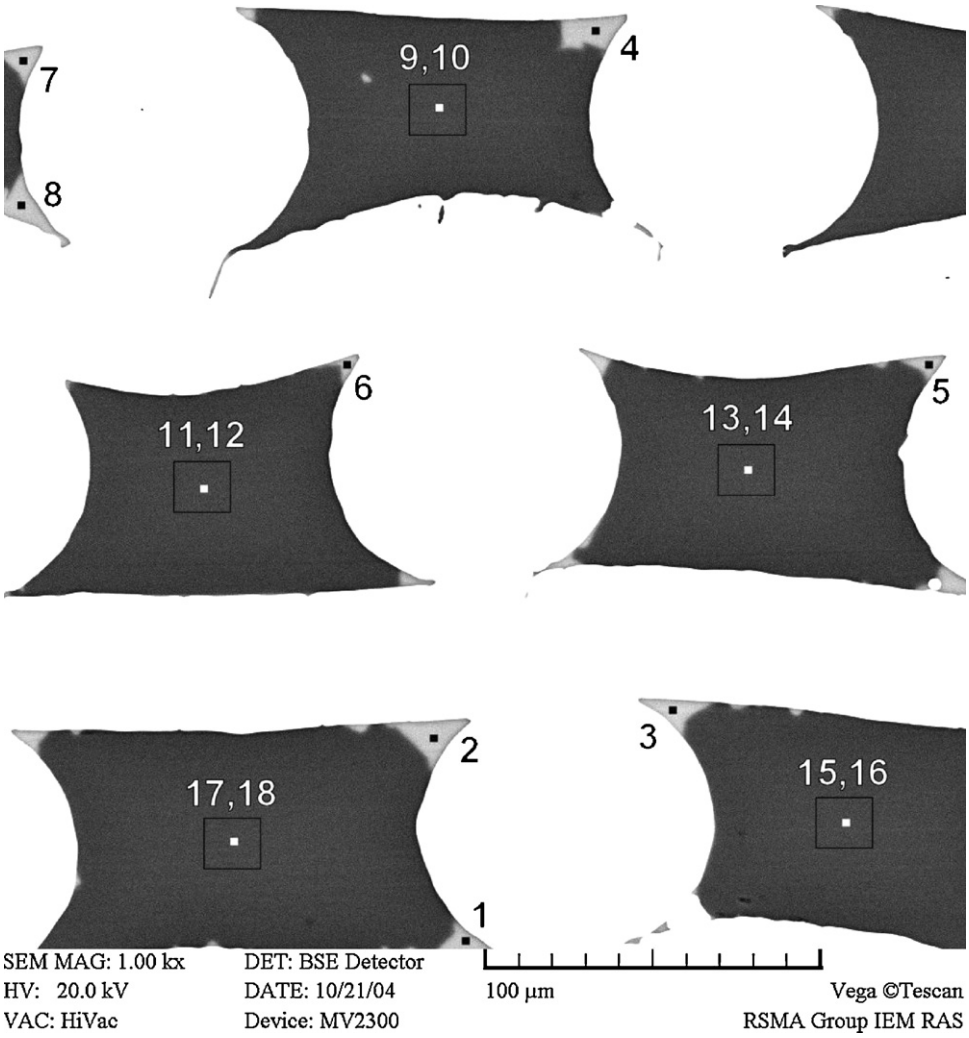

Fig. 3. Typical fibres in a cross-section of a block corresponding to the steady state growth. Black areas are mullite; white ones are g-phase (see details in the text). Block V0566; the cross-section is taken at the middle length of the block. The precursor composition corresponds to $n = 1.8$.

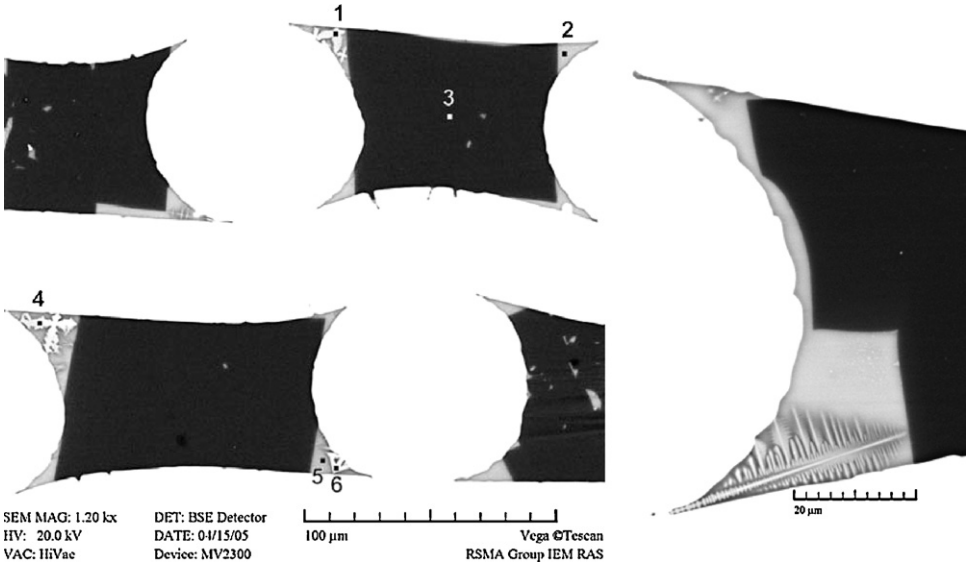

Fig. 4. Typical fibres in a cross-section at the middle length of block V0541 corresponding to the steady state growth. Black areas are mullite; white ones are g-phase (see the text for details). The raw material composition corresponds to $n = 1.5$.

and energy dispersive X-ray (EDX) spectrometer with semiconductor detector INCA Energy 200, was used to study the microstructures of the materials under investigation.

An analysis of the result obtained with the X-ray spectrometer was done by using special software, INCA Energy 200, supplemented by a software developed in Institute of Experimental Mineralogy of RAS.

All the measurements and observations were done at the acceleration voltage of 20 kV. The current of absorbed electrons on a reference sample of Co was equal to (540–620) × 10^{-12} A. The size of electron probe on the sample surface was 157–200 nm; both diameter and depth of the excitation band of the characteristic X-ray radiation are substantially larger. These sizes are decreasing with increasing the average atomic number of a material at a site of the analysis and are increasing with increasing the accelerating voltage. In mullite ($\langle Z \rangle = 10.6$), a characteristic size of the excitation band of a characteristic X-ray radiation at accelerating voltage equal to 20 kV is about 10 μm.

In some cases, the micrographs of specimens in SE and BSE were taken at the current less then 10–12 pA, which allowed getting the resolution of 10–30 nm.

3.2. Microstructures arose as a result of the steady state growth

Typical cross-sections of three oxide/molybdenum blocks corresponding to various values of n are presented in Figs. 1–4.

Consider first a fibre obtained from the raw mixtures corresponding to $n = 2.05$ (Figs. 1 and 2). It should be noted that this particular oxide/molybdenum block was analysed after creep testing at 1500 °C for 386 h (see below). A cross-section of the block shown in Fig. 1 reveals an important feature of the microstructure that is a difference in the microstructure of the central part of the block, which occupies nearly the whole cross-section, and that of fibres located in a periphery of the block. The fibres in the central part look nearly homogeneous, those on the periphery are not homogeneous.

X-ray microanalysis shows that the black phase in SEM-pictures (the first seven rows of Table 1) has atomic ratio Al/Si slightly higher than that in the precursor ($n = 2.05$). Fibres on the very periphery of the oxide/molybdenum block have compositions with an excess of alumina (see the last three rows in Table 1); they are actually composed of a mixture of alumina and mullite. This can be a result of evaporation of silica through rough defects in the molybdenum carcass during the infiltration of the carcass with the alumina/silica melt as the value of saturated pressure of it is higher than that of alumina. The melt in channels located in the central part of the carcass, which occupies the main portion of the cross-section, does not suffer in that way. It is important to note that despite of an excess of alumina in a fibre on the average, in the sharp corners of some fibres a "white" phase can be seen. Such phase occurs, for example, in the right bottom corner of the fibre in the top of Fig. 2.

With the value of n decreasing, an excess of silica in the raw material yields larger areas occupied by the "white" phase (Figs. 3 and 4). The chemical composition of this phase is given in Tables 2 and 3. The "white" phase occurs to be enriched with silica and it is certainly a glassy phase denoted as g-phase further on. Again, a composition of the "black" phase corresponds to mullite. Impurities contents in the two phases of the fibres of block V0566 (see Tables 2 and 4) indicate that the surface of a growing mullite crystal pushes the impurities, which exist

Table 1
Results of the X-ray microanalysis of the fibres presented in Figs. 1 and 2 expressed in atomic ratio Al/Si

Sites in micrographs	Size of the area analysed (μm²)	Al/Si
Fig. 1: Central part	2350 × 2350	4.13
Fig. 2: Spectrum 3	The whole fibres	4.2
Fig. 2: Spectrum 1	43 × 46	4.6
Fig. 2: Spectrum 5	"Point"	4.4
Fig. 2: Spectrum 4	The whole fibres	4.0
Fig. 2: Spectrum 2	47 × 46	4.3
Fig. 2: Spectrum 6	"Point"	4.4
Fig. 1: Periphery, part marked V0762-10	93 × 67	7.8
Fig. 1: Periphery, part marked V0762-11	80 × 67	7.4
Fig. 1: Periphery, part marked V0762-8	74 × 61	7.0

Table 2
Results of the X-ray microanalysis of a g-phase (in atomic per cents) in the fibres shown in Fig. 3

Sites in micrographs	Na	Mg	Al	Si	Ca	Fe	Y	Zr	Al/Si
1	1.24	3.45	10.95	18.64	0.23	0.08	2.31	0.44	0.58
2	0.98	3.44	11.06	18.68	0.28	0.07	2.36	0.38	0.59
3	1.08	3.76	10.40	18.86	0.23	0.07	2.54	0.36	0.55
4	0.99	3.77	10.90	18.72	0.24	0.1	2.27	0.34	0.58
5	1.19	3.48	10.82	19.00	0.23	0.11	2.17	0.34	0.56
6	1.09	3.80	12.26	17.70	0.22	0.07	2.02	0.25	0.69
7	0.99	4.06	10.63	18.63	0.17	0.05	2.5	0.35	0.57
8	0.95	3.78	10.94	18.53	0.24	0.06	2.48	0.41	0.59
Average	1.06	3.69	10.99	18.59	0.23	0.07	2.33	0.36	0.59

Table 3
Results of the X-ray microanalysis of the fibres shown in Fig. 4

Site in micrographs	Na	Mg	Al	Si	Ca	Cr	Fe	Y	Zr	Al/Si
1	0.00	0.23	25.50	0.47	0.04	0.88	13.97	0.00	0.00	
2	0.60	0.00	8.28	18.63	0.10	0.03	10.53	0.06	0.03	0.444
3	0.02	0.00	30.56	7.75	0.00	0.00	0.00	0.03	0.01	3.943
4	0.05	0.00	24.65	0.30	0.02	1.51	14.4	0.00	0.02	
5	0.65	0.16	8.10	19.74	0.10	0.04	9.05	0.02	0.00	0.41
6	0.14	0.11	22.43	1.96	0.04	2.06	13.27	0.00	0.06	

Table 4
Results of the X-ray microanalysis of a "black" phase (in atomic per cents) in the fibres shown in Fig. 3

Sites in micrographs	Na	Mg	Al	Si	Ca	Fe	Y	Zr	Al/Si
9	0.06	0.03	30.45	7.85	0.00	0.00	0.03	0.01	3.88
10	**0.01**	**0.00**	**30.4**	**7.91**	**0.05**	**0.00**	**0.05**	**0.02**	**3.84**
11	0.09	0.04	30.44	7.79	0.03	0.00	0.04	0.01	3.91
12	**0.04**	**0.00**	**30.66**	**7.69**	**0.01**	**0.00**	**0.00**	**0.01**	**3.99**
13	0.12	0.01	30.88	7.41	0.00	0.00	0.04	0.05	4.17
14	**0.05**	**0.01**	**31.12**	**7.26**	**0.01**	**0.00**	**0.01**	**0.03**	**4.29**
15	0.00	0.02	30.58	7.80	0.00	0.00	0.00	0.00	3.92
16	**0.09**	**0.00**	**30.6**	**7.72**	**0.02**	**0.00**	**0.00**	**0.03**	**3.96**
17	0.03	0.01	30.91	7.50	0.04	0.00	0.00	0.00	4.12
18	**0.05**	**0.03**	**30.61**	**7.63**	**0.04**	**0.04**	**0.01**	**0.02**	**4.01**
Average	0.05	0.01	30.66	7.66	0.00	0.00	0.02	0.02	4.01

Bold digits are used for the results obtained by scanning squares marked in Fig. 3.

in the melt, to a silica enriched melt that solidifies at a lower temperature to form inclusions of the g-phase. Normally these inclusions are located in coldest zones of a channel in the molybdenum carcass. Solidification of the g-phase can be accompanied with crystallisation of dendrites, see Fig. 4. In the vicinity of a dendrite, gradients of the grey colour are observed (see the insertion of a micrograph of a higher magnification in Fig. 4). This is certainly an evidence of redistribution of the contamination elements between the phases just prior formation of the dendrites and during solidification of the g-phase.

The microphotographs and the Tables presented reveal some important features of the fibre microstructures:

1. The composition of mullite in the fibres is close to $2Al_2O_3$:SiO_2 independent of the initial composition of the precursor. Deviation from the exact molar ratio, 2:1, does not contradict to a rather broad field of the existence of mullite in various phase diagrams published.
2. Mullite is optically transparent, which is characteristic to single crystal. The content of impurities in the mullite phase does not reach the sensitivity of the experimental method.
3. Inclusions of the glassy phase are located mainly at the fibre periphery, preferably in the sharp corners of the fibre cross-section. These sites are the coolest in a cross-section of a block during the fibre crystallisation due to high thermal conductivity of molybdenum. In the crystallisation process mullite pushes out contamination to the glassy phase, which solidifies later at lower temperature.

3.3. Initial stage of the fibre growth

Crystallisation of the fibres of simple oxides, such as sapphire, in the ICM-process starts with spontaneous crystallisation of the overcooled melt at the top of an oxide/molybdenum block yielding a set of polycrystalline fibres in the channels. Then crystals emerged at the solid/liquid boundary serve as seeds for the rest of the liquid columns to determine the crystallographic orientation of the fibres provided a characteristic cross-sectional size of the channels is sufficiently small (see Fig. 14.4 in[12] and a discussion around it). Crystallisation of mullite fibres is similar to that in some details and different from it in other details. Observing changes of the microstructure of mullite fibres crystallised from the melts with $n<2$ along the length of a block provides an insight into the growth mechanisms of mullite that yield a microstructure of the fibre considered in the previous section.

The microstructure of fibres at the top of an oxide/molybdenum block is presented in Fig. 5. One can clearly see a number of the mullite crystals divided by silica-based phase in a channel. For example, in an area marked by a circle, three crystals are seen. The direction of all crystals along the fibre axis coincides certainly with *c*-axis of the mullite crystal. However, their angular orientations can vary.

Crystallisation proceeds with growing some crystals of various angular orientations. The process is accompanied with pushing a liquid, which is to form the glassy phase, towards the oxide/molybdenum interface. An intermediate microstructure is presented in Fig. 6 (the micrograph in the bottom of the figure): a number of the crystals is much lower than at the top of the block, the glassy phase inclusions are becoming larger and have moved closer to the fibre surface. The final stage, a steady growth, yields the microstructures shown in Figs. 1–4.

Obviously, kinetic of the crystallisation process depends on many parameters such as pulling rate, temperature gradients,

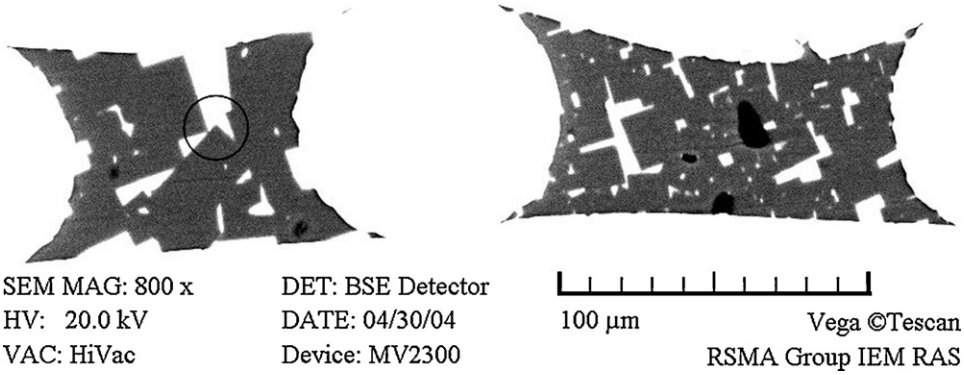

Fig. 5. The microstructure of fibres in a cross-section of block V0541 ($n=1.5$), the same as in Fig. 4. The cross-section is taken at a distance of 5 mm from the top of the block.

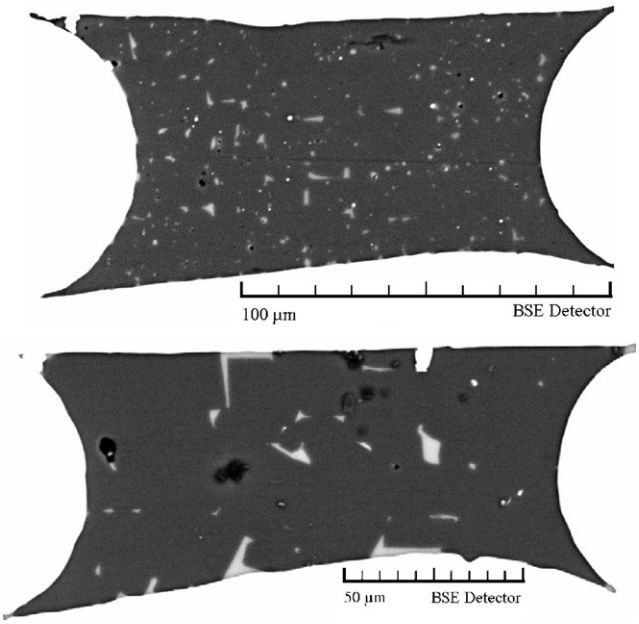

Fig. 6. The microstructure of the fibres in a cross-section of block V0566 ($n = 1.8$), the same as in Fig. 3, taken at a distance of 5 mm (the top image) and 20 mm (the bottom image) from the top of the block.

melt composition, etc. The dependencies are remained to be analysed that will yield an optimisation of the technological process.

4. Creep resistance

Mullite as a base of high temperature materials is an attractive substance, first of all, because of its high creep resistance.[1] Hence, measuring creep resistance of mullite fibres is a problem of the primary importance.

4.1. Methodology

It is convenient to load fibres produced by the internal crystallisation method without taken them from molybdenum matrix, that means testing oxide-fibre/molybdenum-matrix composites and then calculating creep properties of the fibres. Also it is convenient to test composite specimens by loading them in bending.

A composite is assumed to be characterised by identical creep behaviour under tension and compression and the creep law of the material is

$$\dot{\varepsilon} = \eta_n \left(\frac{\sigma}{\sigma_n} \right)^n \tag{1}$$

where n and σ_n are constants and value of η_n is chosen arbitrary; it is convenient to take $\eta_n = 10^{-4}\,\mathrm{h}^{-1}$, which means that σ_n is the stress to cause 1% creep strain for 100 h. We call this value as creep resistance of a material on 100-h time base.

A solution of a creep problem for a beam under bending yields a dependence of the deflection rate, $\dot{f}$, of the beam at its centre on applied load Q. For a beam of rectangular cross-section of height $2h$, width b we have:[15]

$$\dot{f} = \eta_n \frac{1}{2^{3n+2} n^n (n+2)} \left(\frac{Q}{\sigma_n h^2} \right)^n \left(\frac{L}{b} \right)^n \left(\frac{L}{h} \right) L \tag{2}$$

for the case of 3-point bending and

$$\dot{f} = \chi_n \left(\frac{M}{M_n} \right)^n \frac{l^2}{8} \tag{3}$$

for the case of 4-point bending. Here

$$M = \frac{Q}{2} \frac{L-l}{2},$$

L and l are the distances between periphery and internal supports, respectively, $\chi_n = \eta_n / h, \quad M_n = (2n/2n+1)\,\sigma_n b h^2$.

Bending tests were performed under a step-wise varying load that yields creep characteristics of the composite in a particular specimen. This allows excluding a number of the factors, which determine a usual scatter of the creep data of a batch of the material.

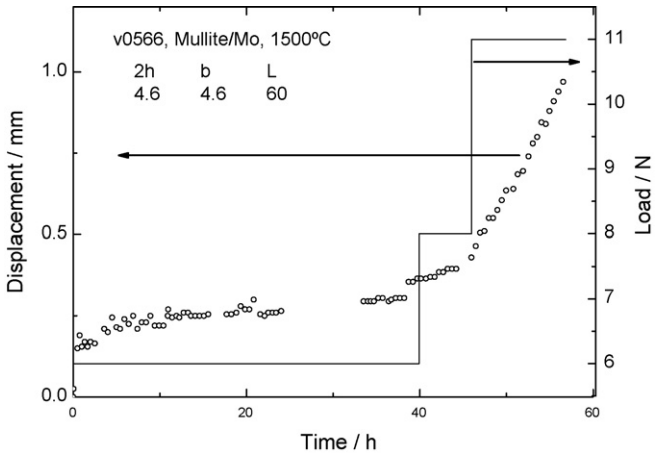

Fig. 7. The displacement vs. time for mullite/molybdenum specimen V0566 (fibre volume fraction is 35%). Specimen sizes ($2h$, b, L) in mm are shown in the graph field.

4.2. Experimental results

The experimental technique is described elsewhere.[16] Original experimental data are obtained as dependencies of the displacement at the specimen centre on the load. An example of the original creep curve is presented in Fig. 7. Dependencies of the steady state displacement rate on applied load yield values of n in a power low of creep, Eq. (1), then using Eqs. (2) and (3) gives values of creep resistance σ_n of an oxide/molybdenum block. Since molybdenum is fully recrystallised during the melt infiltration at a temperature of about 1900 °C, its creep resistance at temperatures 1400 °C and higher is negligible as compared to that of single crystalline oxides.[12] Hence, taking into account oxide volume fraction in a block, which is usually between 35 and 45%, yields the creep resistance of a fibre. The results are presented in Fig. 8 together with the only published long time ago experimental point obtained by loading a bulk crystal by compression and measuring its length after the specimen had

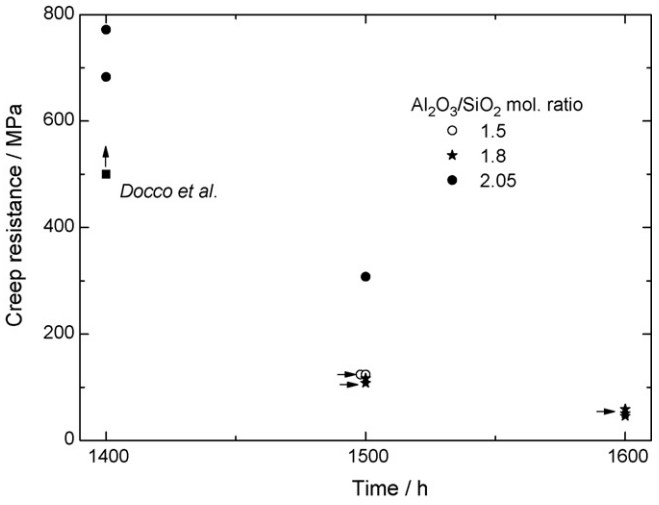

Fig. 8. Creep resistance of mullite fibres crystallised from the precursors with various Al_2O_3/SiO_2 molar ratios. All experimental points are obtained in 3-point bending tests except for the points marked by horizontal arrows, which are the results of 4-point bending tests. Point marked *Docco et al.* are the only one obtained in testing mullite single crystal.[1]

been kept under a constant load for 200 h. One can see that the data obtained in the present work are higher than the estimation by Dokko et al.[1]

At a temperature of 1400 °C the stress to cause 1% of creep strain approaches 800 MPa, which is certainly a highest creep resistance at that temperature ever measured. At 1500 °C the creep resistance decreases down to about 300 MPa. Perhaps, this is affected by the glassy inclusions, which can be softening at that temperature. No doubt, this value can be enhanced by an appropriate choice of fabrication regimes to diminish a volume fraction of the glassy phase.

5. Conclusions

1. Applying the internal crystallisation method to crystallise Al_2O_3:SiO_2 melts corresponding to molar ratios from 1.5 to 2.05 yields two-phase fibres containing single crystalline mullite and glassy silica-based inclusions.
2. Mullite phase has the Al_2O_3/SiO_2 molar ratio close to 2 independent of the molar ration in the precursor.
3. At the starting stage of the crystallisation process, the glassy phase inclusions are small and located rather homogeneously on the fibre cross-section. As the crystallisation proceeds the inclusions are growing and are shifting towards the fibre surface (oxide/molybdenum interface) certainly due to radial temperature gradient existing in each channel. At the steady stage of the process a fibre occurs consisting of single crystalline main body in the central part of the cross-section and glassy inclusions on the surface. With increasing the Al_2O_3/SiO_2 molar ratio of the precursor melt, the volume fraction of the inclusions decreasing. At the molar ration equal to 2.05 the inclusions are still exist, but they are small and located mainly in the sharp corners of some fibres.
4. While crystallizing from the melt containing contaminations, mullite is pushing out impurities to the glassy phase. The mullite phase becomes pure.
5. The presence of the glassy phase yields a decrease in the creep resistance of the fibres. The effect is especially pronounced at temperatures higher than 1500 °C due to melting of the glassy phase. Still, the fibres obtained from the precursor with the Al_2O_3/SiO_2 molar ratio of 2.05 have excellent creep resistance at a temperature of 1400 °C and fairly high creep resistance at 1500 °C.
6. The results obtained form a solid base for developing fabrication technology of single crystalline mullite fibre with high creep resistance at temperatures up to about 1600 °C.

Acknowledgements

The work was performed under financial support of International Science and Technology Centre (Project 2456) and Russian Foundation of Basic Research (Project 06-03-91376). Fruitful discussions with Professor H. Schneider and the help in the experimental work by Mrs. N. Prokopenko, Mr. L. Kozhevnikov, Mr. A. Mizkevich and Mr. A. Nekrasov are also greatly acknowledged.

References

1. Dokko, P. C., Pask, J. A. and Mazdiyasni, K. S., High-temperature mechanical properties of mullite under compression. *J. Am. Ceram. Soc.*, 1977, **60**, 150–155.
2. Kriven, W. M., Schneider, J., Palko, J. W., Sinogeikin, S., Bass, J. D., Sayir, A. *et al.*, High temperature single crystal properties of mullite. *J. Eur. Ceram. Soc.*, 1999, **19**, 2529–2541.
3. Schneider, H., Göring, J., Kanka, B. and Schmücker, M., Whipox: Ein neuer Oxidfaser/Oxidmatrix-Leichtbauwerkstoff für Hochtemperaturanwendungen. *Keram. Z.*, 2001, **53**, 788–791.
4. Braue, W., Borath, R., Flucht, F. and Schneider, H., Failure analysis of NextelTM 720 fibers subjected to high-temperature testing: the role of intrinsic fiber impurities. In *High Temperature Ceramic Matrix Composites*, ed. W. Krenkel, R. Naslain and H. Schneider. Wiley VCH, 2001, pp. 90–95.
5. Wilson, D. M. and Visser, L. R., High performance oxide fibers for metal and ceramic composites. *Compos. Part A*, 2001, **32**, 1143–1153.
6. Sayir, A. and Farmer, S. C., Directionally solidified mullite fibers. ceramic matrix composites: advanced high-temperature structural materials. In *Proceedings of the Materials Research Society Symposium*, *vol. 365*, ed. R. A. Lowden. Materials Research Society, Pittsburgh, PA, 1995, pp. 11–21.
7. Pask, J. A., Importance of starting materials on reactions and phase equilibria in the AI_2O_3–SiO_2 system. *J. Eur. Ceram. Soc.*, 1996, **16**, 101–108.
8. Shornikov, S. I., Archanov, I. Yu. and Ceenova, T. Yu., Mass spectrometric analysis of vapour process and equilibrium in the Al_2O_3–SiO_2 system. *J. Phys. Chem.*, 2000, **74**(5), 775–782 [in Russian].
9. LaBelle Jr., H. E. and Mlavsky, A. I., Growth of sapphire filaments from the melt. *Nature*, 1967, **216**, 574–575.
10. Burrus, C. A. and Coldren, L. A., Growth of single-crystal sapphire-clad ruby fibers. *Appl. Phys. Lett.*, 1977, **31**(6), 383–384.
11. Mileiko, S. T. and Kazmin, V. I., Crystallization of fibres inside a matrix: a new way of fabrication of composites. *J. Mater. Sci.*, 1992, **27**, 2165–2172.
12. Mileiko, S. T., *Metal and Ceramic Based Composites*. Elsevier, Amsterdam, 1997.

13. Mileiko, S. T., Kiiko, V. M., Starostin, M. Yu., Kolchin, A. A. and Kozhevnikov, L. S., Fabrication and some properties of single crystalline mullite fibers. *Scripta Mater.*, 2001, **44**, 249–255.
14. Rüscher, C. H., Mileiko, S. T. and Schneider, H., Mullite single crystal fibers produced by the internal crystallization method (ICM). *J. Eur. Ceram. Soc.*, 2003, **23**, 3113–3117.
15. Mileiko, S. T., Oxide-fibre/Ni-based matrix composites—III: a creep model and analysis of experimental data. *J. Compos. Sci. Technol.*, 2002, **62**(2), 195–204.
16. Mileiko, S. T. and Kiiko, V. M., High temperature creep of metal matrix composites under variable loadings. *Mech. Compos. Mater.*, 2004, **40**(4), 523–534 [in Russian].